JOURNAL OF THERMOPHYSICS AND HEAT TRANSFER
Vol. 10, No. 2, April–June 1996

Effective Emittance for Cassini Multilayer Insulation Blankets and Heat Loss near Seams

Edward I. Lin,* James W. Stultz,* and Ronald T. Reeve†
Jet Propulsion Laboratory, California Institute of Technology, Pasadena, California 91109

Thermal performance of Cassini multilayer insulation (MLI) blankets was characterized in thermal vacuum tests. Effective emittance was derived for the standard and high-temperature layups, with or without micrometeoroid protection standoffs, and for a high-performance duo-layup with staggered seams. The all-Kapton® layup was shown to have a 19% higher effective emittance than the hybrid Kapton–Mylar® layup, and the duo-layup exhibited a dramatic capability of reducing heat dissipation by 2.6-fold. Several different definitions of effective emittance are discussed, and their relations to distinct hardware–MLI configurations and corresponding modeling techniques clarified. Large temperature differences (up to 70°C) were observed between the center and seam of a blanket. Heat losses in the vicinity of seams are quantified, and a major MLI heat loss mechanism elucidated.

Nomenclature

A = area of radiating surface, m^2
G = radiation conductor, W/°C[4]
Q = heat dissipation rate, W
T_C = temperature on the cold side, °C
T_H = temperature on the hot side, °C
ε_{eff} = effective emittance
σ = Stefan–Boltzmann constant

Subscripts
ho = hardware to outer layer of MLI
hs = hardware to sink
hwr = hardware
i = inner layer of MLI
io = inner to outer layer of MLI
o = outer layer of MLI

Introduction

MULTILAYER insulation (MLI) blankets perform a critical function in maintaining spacecraft components within required temperature limits in the extreme hot and cold environments of space. Several decades of analytical and test work have yielded an extensive body of knowledge regarding MLI blanket design and performance.[1–3] However, occasions do arise from time to time where the existing database does not provide answers to specific questions, and a special investigation becomes necessary. A case in point is the MLI blankets for the Cassini spacecraft.

The Cassini spacecraft is being developed for a mission to explore Saturn and its rings, satellites, and magnetosphere. The scheduled 1997 launch will take the spacecraft through a Venus–Venus–Earth–Jupiter gravity assist (VVEJGA) trajectory, subjecting it to a 0.61 astronomical unit (AU) high-temperature environment at perihelion. Temperatures on some sunlit blanket surfaces at 0.61 AU can reach levels that are beyond the service capability of the conventional Mylar/Dacron® net MLI. For example, the radioisotope thermoelectric generator (RTG) shade MLI temperature is predicted to be around 300°C under the combined heating of the RTG (3900 W) and 2.7 suns (i.e., at 0.61 AU) during a trajectory correction maneuver. The main engine blanket temperature can reach 360°C during engine firing in conjunction with the 0.61 AU solar illumination. The majority of the blanket surfaces, however, will experience temperatures with an upper bound of 250°C, since the spacecraft will cruise in the shade of its high-gain antenna, which is sun-pointed most of the time.

These worst-case hot Cassini MLI temperature predictions are significantly higher than those expected for previous spacecraft, e.g., the Galileo. To cope with the high-temperature environment, the baseline Cassini MLI design includes a standard layup and a high-temperature layup. The high-temperature layup consists of 20 layers of embossed Kapton with a black Kapton outerlayer, and will be used only at locations of extremely high temperatures, such as in the vicinity of the RTG and the main engine. The standard layup is a hybrid consisting of 5 layers of embossed Kapton and 15 layers of Mylar/Dacron net with appropriate outer and inner layers, and will be used at over 85% of the blanketed surfaces on the spacecraft.

The high-temperature survivability of these layups has been successfully demonstrated in a series of high-temperature exposure tests that employed a 2.7-sun solar simulator.[4] However, the thermal performance of these layups, specifically their effective emittance in several hardware configurations, has not been characterized before. For example, while experience and intuition suggested that the all-Kapton layup would be leakier (i.e., have higher effective emittance) than the conventional Mylar/Dacron net-type construction because of greater interlayer contact and greater susceptibility to local compression, no effective emittance data existed to provide a convincing comparison. In addition, because of micrometeoroid protection requirements, MLI blankets at numerous locations are spaced off the hardware by 3.81 or 6.35 cm with Mylar standoffs. Elsewhere, they are either closely wrapped around the hardware, or are installed in a tent-like configuration. It has been found that the manner of blanket installation significantly determines the method of modeling, which in turn invokes the appropriate definition of MLI effective emittance. This was not previously discussed in the literature, yet this has important consequence in terms of the values to be used for the effective emittance, as well as the temperatures that result from the analysis.

Presented as Paper 95-2015 at the AIAA 30th Thermophysics Conference, San Diego, CA, June 19–22, 1995; received July 3, 1995; revision received Dec. 11, 1995; accepted for publication Dec. 14, 1995.

*Member of Technical Staff, Mechanical Systems Engineering and Research Division, 4800 Oak Grove Drive. Member AIAA.

†Technical Group Supervisor, Mechanical Systems Engineering and Research Division, 4800 Oak Grove Drive.

This article will start by presenting some fundamental considerations related to various definitions of MLI effective emittance, and the associated techniques of thermal modeling. A description of the test articles, setup, and procedure will then follow. The test results will be analyzed, yielding effective emittance data applicable in various situations. As a bonus from the test program, the heat loss characteristics in the vicinity of blanket seams will be discussed. Finally, a method of fabricating high-performance MLI blanket will be validated, complete with quantitative performance characterization.

Effective Emittance

The effective emittance of an MLI blanket is mathematically defined as

$$\varepsilon_{\text{eff}} = Q/A\sigma(T_H^4 - T_C^4) \tag{1}$$

Several interpretations of this equation are possible depending on what T_H and T_C are taken to be. This is directly related to how the analyst models the hardware, and it determines what value the analyst should use for the MLI effective emittance. This is not always clear in thermal analysis and the reporting of effective emittance in the literature usually does not make any distinction among the various interpretations. Thus, significant errors sometimes result. The following three definitions of ε_{eff} are encountered in the Cassini thermal design, each relevant to a particular hardware–blanket configuration:

$$\varepsilon_{\text{eff}} \equiv \varepsilon_{\text{eff-hs}} \text{ if } A = A_{\text{hardware}},\ T_H = T_{\text{hardware}} \text{ and } T_C = T_{\text{sink}} \tag{2}$$

$$\varepsilon_{\text{eff}} \equiv \varepsilon_{\text{eff-ho}} \text{ if } A = A_{\text{hardware}},\ T_H = T_{\text{hardware}} \text{ and } T_C = T_{\text{outer-layer}} \tag{3}$$

$$\varepsilon_{\text{eff}} \equiv \varepsilon_{\text{eff-io}} \text{ if } A = A_{\text{MLI}},\ T_H = T_{\text{inner-layer}} \text{ and } T_C = T_{\text{outer-layer}} \tag{4}$$

Figure 1 illustrates the three hardware–MLI configurations that call for modeling techniques invoking the previous three definitions for effective emittance. Figure 1a involves wrapping the MLI blanket snugly around the hardware. Figure 1b involves applying micrometeoroid-protection standoffs between the MLI blanket and the hardware; e.g., Cassini employs Mylar accordion strips of 3.81 or 6.35 cm height to alleviate the impact of micrometeoroids on sensitive hardware. Figure 1c involves draping the MLI blanket over the hardware in a tent-like manner, leaving a substantial distance between the blanket and the hardware; Cassini has several such applications, e.g., for the fields and particles pallet (FPP) and the propulsion module subsystem (PMS).

Note that modeling technique Fig. 1a requires, in addition to $\varepsilon_{\text{eff-hs}}$, an effective solar absorptance that depends on the solar absorptivity of the MLI outer layer as well as the effective emittance of the MLI. In contrast, modeling technique Fig. 1b uses directly the emissivity and solar absorptivity of the MLI outer layer. Therefore, while modeling technique Fig. 1a is still being practiced, it is often replaced by modeling technique Fig. 1b, which has an additional advantage of yielding the outer layer temperature automatically.

A mathematical relationship exists linking the previous three definitions of effective emittance. However, its derivation and related theoretical discussion requires substantial space and will be considered elsewhere.

Test Articles, Setup, and Procedure

Test Articles

Blanketed Boxes

MLI blankets were tested in pairs, each wrapping around a 22.86 × 22.86 × 22.86 cm aluminum box that was heated from within. Figure 2 depicts the aluminum box on the right and an MLI blanket on the left. The box, which has Mylar standoffs on it, was inserted in the blanket, and the open flap of the blanket was laced closed, then the blanketed box was installed in the vacuum chamber for testing. Figure 3 depicts a pair of blanketed boxes ready for installation in the vacuum chamber.

The identical boxes were made from 0.318-cm-thick aluminum 6061-T6 plates. The inside of the boxes was painted black (to help achieve a uniform box temperature) and the outside left as machined. Thermofoil heaters and thermocouples were mounted on the inside of each of the six panels. The top and four side panels were welded together, but the bottom panel (with a 0.953-cm-diam hole at the center) was bolted to the bottom edges of the four side panels with eight no. 10

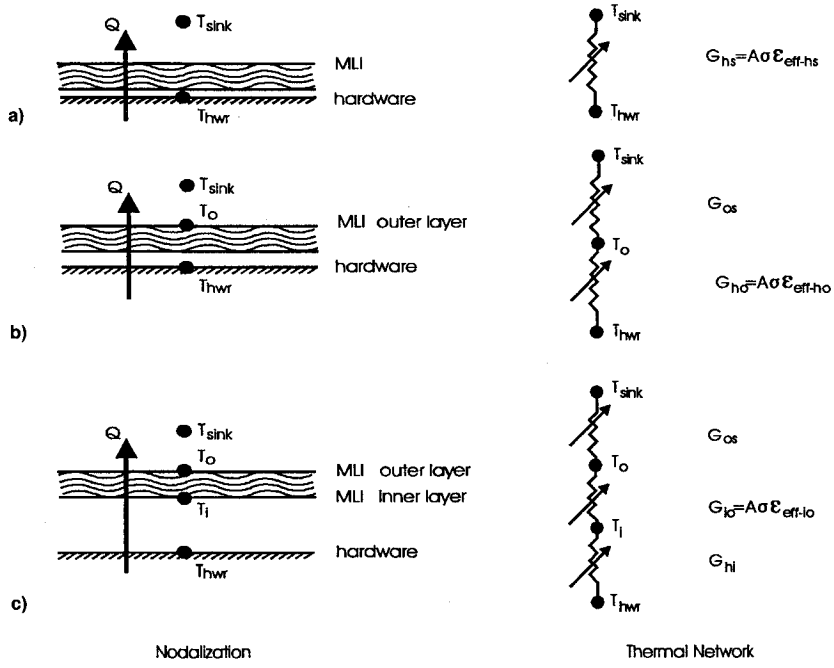

Fig. 1 Modeling of three different hardware–MLI configurations and the associated ε_{eff} definitions.

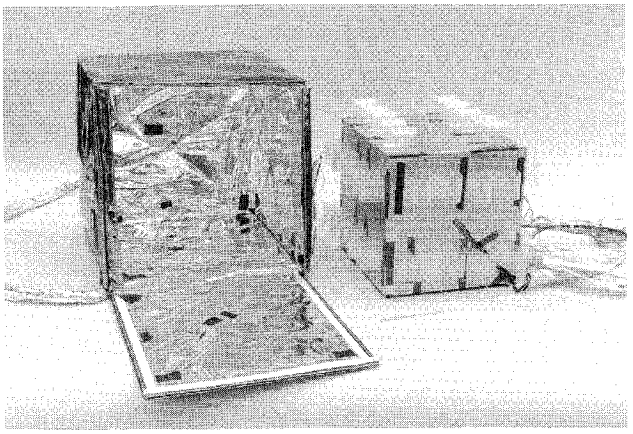

Fig. 2 MLI blanket and aluminum box with Mylar standoffs.

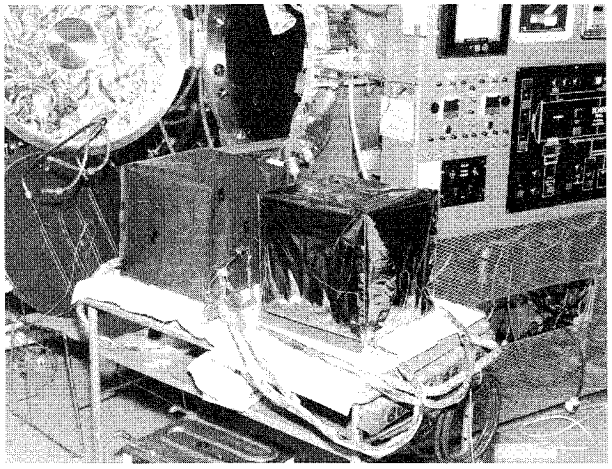

Fig. 3 Pair of blanketed boxes ready to be installed in chamber.

bolts. Wires from the heaters and thermocouples were routed out through the center hole, and the bottom panel was secured after all instrumentation inside the box was completed.

MLI Blankets

Four MLI blankets were tested. Their designations and layup designs are as follows:

MLI-A: SSAK + 5EK + 15MN + AK, with micrometeoroid standoffs (the standard layup).

MLI-B: BK + 20EK + AK, with micrometeoroid standoffs (the high-temperature layup).

MLI-C: SSAK + 5EK + 15MN + AK, no micrometeoroid standoffs.

MLI-D: Outer blanket layup SSAK + 5EK, inner blanket layup 15MN + AK, seams staggered, with micrometeoroid standoffs.

The blanket constituents referred to previously are as follows:

SSAK: Second surface aluminized Kapton, $\frac{1}{2}$ mil thick, ITO (indium tin oxide) coated on the front, Nomex scrim reinforced on the back, used for outer layer.

BK: Black Kapton, carbon-filled, 1 mil thick, used for outer layer.

EK: Embossed Kapton, $\frac{1}{3}$ mil thick, aluminized on both sides, used for intermediate layer.

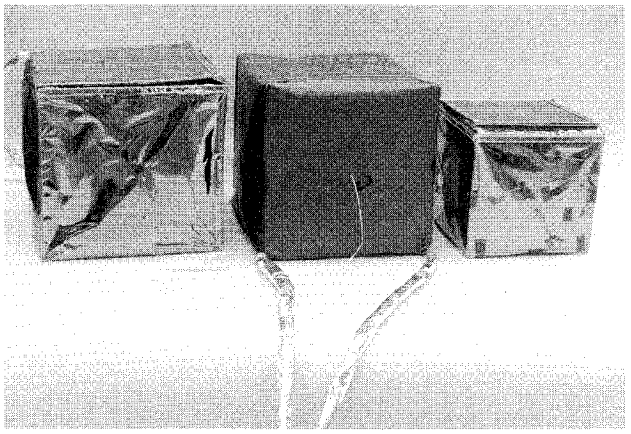

Fig. 4 Photographs of MLI-A, MLI-B, and MLI-C.

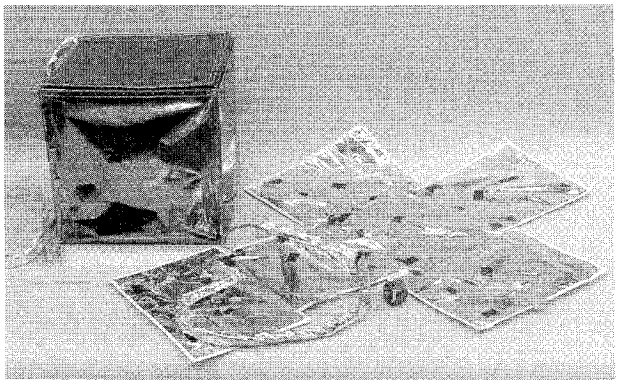

Fig. 5 Photograph of MLI-D.

MN: Mylar with Dacron net, alternating layers; $\frac{1}{4}$ mil thick, Mylar aluminized on both sides, used for intermediate layer.

AK: Aluminized Kapton, 1 mil thick, aluminized on both sides, used for inner layer.

Photographs of MLI-A, MLI-B, and MLI-C are shown in Fig. 4, from left to right. A photograph of MLI-D is displayed in Fig. 5, with the outer blanket being box-shaped on the left, and the inner blanket unfolded on the right. MLI-A, -B, and -D are of dimensions 31.53 cm cubed, while MLI-C is 23.92 cm cubed.

Instrumentation

Thermofoil heaters were mounted on the interior of the boxes, two on each face, with large area coverage to help achieve uniform heating of the boxes. All thermocouples were of type E (Chromel constantan), gauge 30, and with a copper tab. Fourteen thermocouples were affixed to the interior of each box, the guideline being one thermocouple at the center of each face, and one near each corner of the box.

Thermocouple placement on the blankets followed the same guideline. Thermocouples on the inner and outer layers were paired so that they were directly opposite each other. No thermocouples were placed on the intermediate layers. Typically, each blanket used a total of 28 thermocouples. The chamber shrouds were also provided with thermocouples so that temperatures around the test boxes were monitored.

A guard heater was mounted on the 20 wires that exited the center hole on the bottom plate of each box to control heat loss to under 0.05 W. Eight dc power supplies were employed, three for each of the two boxes and one for each of the two guard heaters. The Space Simulator System at JPL's Environmental Test Lab was utilized for data acquisition and power control.

Test Setup

The tests were conducted in chamber no. 20 at the Environmental Test Lab. The chamber has internal shroud dimensions of 68.58 cm diam by 91.44 cm length. Figure 3 shows the chamber in the background. During installation of the test articles, the boxes were suspended from the chamber top rail with a stainless-steel wire, and were anchored to the chamber walls by three Nomex chords to prevent their movement and rotation (the stainless-steel wire and Nomex® chords conducted very little heat and are visible in Fig. 3). An LN_2-cooled cold plate (seen to the left of Fig. 3, below the chamber door) was employed to separate the two boxes, thereby dividing the chamber into two almost identically conditioned compartments. The cold plate was converted from a used heat exchanger plate and was painted black on both sides. The door shroud was also painted black on the inside and was covered with a 20-layer MLI on the outside to ensure that extraneous heat input from outside the chamber was minimized. The goal of the arrangement was that all sides of the two boxes were viewing surfaces at essentially the same temperatures.

Test Procedure

There were three test phases: phase 1 involved MLI-A and MLI-C, phase 2 involved MLI-A and MLI-B, and phase 3 involved MLI-A and MLI-D. Each phase was conducted in a vacuum of less than 1×10^{-5} torr, and with the chamber shrouds and cold plate controlled first to the LN_2 temperature (−185°C), then to −100°C, approximately. The box temperatures were targeted to be around 20 and 50°C, respectively, to simulate a nominal and a hot hardware condition. The heater power required per box for each set of conditions was first estimated, then fine-tuned during the test. For each test phase, following the chamber pump down, the power supply was brought up to a level suitably greater than the intended one, dropping to the intended level only after the box temperature had approached the target value. This overshooting and slow coasting down technique was employed to speed up the process of attaining steady state, and needed to be practiced with some art. Steady state was regarded as achieved if temperatures changed at a rate of no greater than 0.2°C/h.

After each test phase, which consisted of three or four stages, was completed, a chamber break would occur, the boxes would be removed from the chamber, and a new pair of blankets would replace the pair just tested. Then the process of testing would be repeated.

Test Results and Effective Emittance

The test data recorded during the three test phases are presented in Table 1. They are power required Q to maintain the box temperature T_b, the MLI outer and inner layer temperatures, T_o and T_i, respectively, at the given chamber shroud temperature T_s. Temperatures T_b, T_s, T_o, and T_i are averaged values. The box and shroud temperatures do not vary more than 2 or 3%, but the MLI center and corner temperatures differ substantially. For this reason, both T_o and T_i are listed in Table 1, first as the average of the six center temperatures, then on a separate line as the average of the eight corner temperatures, for every test case. In general, center temperatures vary less than corner temperatures; on occasions, some corner temperatures may appear erratically different from the rest of the same MLI. Overall, however, the averaging scheme appears to be quite reasonable, and the effective emittances calculated corroborate with each other very well.

Since the test articles and test setup were designed so that heat losses via the supporting wires and thermocouple and heater wires were negligible, the power input to the boxes is assumed to be completely dissipated through the MLI. Applying Eqs. (1–4), these test data were used to calculate $\varepsilon_{\text{eff-hs}}$, $\varepsilon_{\text{eff-bo}}$, and $\varepsilon_{\text{eff-io}}$. The calculated effective emittances are presented in Table 1.

Comparison of Layups and Effect of Standoff

As can be seen in Table 1, $\varepsilon_{\text{eff-hs}}$, which is sometimes called the traditional effective emittance, appears to be unambiguously determined for all four blanket layups. The average value is 0.026 for MLI-A (the standard layup), 0.031 for MLI-B (the high-temperature layup), 0.024 for MLI-C (the standard layup without standoffs), and 0.010 for MLI-D (the duo-blanket with staggered seams). Note that the 0.026 value agrees well with the initial Cassini design guideline of 0.02 ± 0.005 for this size and type of blanket. Also note that deviations of all data from these averages are relatively small. In fact, considering that four different MLI layups were involved in three different test phases, that chamber breaks and rearrangement of test articles occurred between test phases, and that the tests were conducted at several temperature settings, these results exhibit a rather high degree of repeatability.

It is significant that the effective emittance for MLI-B, the all-embossed Kapton layup, is 19% higher than that for MLI-A, the hybrid Kapton–Mylar layup. This gives credence to and quantifies the intuitive feel that many had shared before the test. It is also interesting to note that the effective emittance for MLI-C is 8% lower than that for MLI-A. Both are of the same hybrid Kapton–Mylar layup, yet the tighter fit of MLI-C (less blanket area) as a result of the absence of the micrometeoroid standoffs, actually is able to keep the box warmer. A close comparison between results for test phases 1a–1d for the two blankets shows that MLI-C kept the box about 2°C warmer although using less power. Finally, it is highly significant that the effective emittance for MLI-D is 2.6 times lower than that for MLI-A. This demonstrates that the technique of duo-layup and staggering seams is able to cut down heat dissipation dramatically. (Note that the seaming technique is the same for all four blankets; MLI-D differs from the rest in that seams for its inner and outer blankets are staggered so that through seams are eliminated.) The underlying reason for this superior performance will be explained later in this article.

Hardware-to-Outerlayer Effective Emittance

Table 1 shows that $\varepsilon_{\text{eff-ho}}$ and $\varepsilon_{\text{eff-hs}}$ are almost identical. This is so because the radiation resistance from the outer layer to the sink is much less (roughly 10–40 times) than that from the hardware to the outer layer. This explains why applying $\varepsilon_{\text{eff-hs}}$ in the modeling scheme shown in Fig. 1b, as is often done in spite of being a mismatch, does not cause significant errors. It is believed that most effective emittance data reported in the literature are $\varepsilon_{\text{eff-hs}}$, although in most cases this is not specified. Also, whether the outer layer temperature is identified with that of the center, corner, or some average of the two, the value of the computed $\varepsilon_{\text{eff-ho}}$ is hardly affected.

Intrinsic MLI Effective Emittance

As Table 1 clearly indicates, $\varepsilon_{\text{eff-io}}$ is very different from $\varepsilon_{\text{eff-hs}}$. In the hardware–MLI configuration in Fig. 1c, if the modeling uses $\varepsilon_{\text{eff-hs}}$ instead of the correct $\varepsilon_{\text{eff-io}}$, substantial errors will result. Both $\varepsilon_{\text{eff-hs}}$ and $\varepsilon_{\text{eff-io}}$ have entered discussions in the MLI literature, but usually without a clear distinction between the two. These results show that a clear distinction is necessary. Physically, the effective emittance based on the inner- and outer-layer temperatures is an intrinsic characteristic of the blanket layup, while the traditional effective emittance also incorporates effects of the hardware surface emissivity, the MLI inner- and outer-layer emissivity, the hardware-to-blanket gap geometry, the standoffs if any, and the emissivity and geometry of the chamber shroud. The latter includes the various surface resistances and space resistances, and hence, is expected to be lower than the former.

However, this is just the opposite of what Table 1 indicates, that $\varepsilon_{\text{eff-hs}}$ is significantly higher than $\varepsilon_{\text{eff-io}}$ in most cases. The apparent paradox is the result of applying the appropriate area in the calculation of ε_{eff} using Eqs. (1–4). As noted in Table 1, $\varepsilon_{\text{eff-hs}}$ is based on A_{hwr}, which is equal to 0.314 m^2, but $\varepsilon_{\text{eff-io}}$

Table 1 Cassini MLI test results and computation of effective emittance[a]

Thermal blanket	Test phase[b]	Q, W	T_h, °C	T_s, °C	$E_{\text{eff-hs}}$, w/A_{hwr}	T_o, °C	T_i, °C	$E_{\text{eff-ho}}$, w/A_{hwr}	$E_{\text{eff-io}}$, w/A(MLI)
MLI-A	1a	3.449	20.4	−186.9	0.026	−173.5	8.8	0.026	0.016
						−149.1	2.5	0.027	0.018
	1b	5.205	54.6	−186.5	0.026	−170.6	43.2	0.026	0.016
						−142.8	36.9	0.026	0.017
	1c	4.733	54.7	−102.2	0.025	−102.5	44.5	0.025	0.015
						−96.8	40.8	0.025	0.016
	1d	2.998	22.3	−104.6	0.025	−103.4	12.4	0.025	0.015
						−99.3	7.3	0.025	0.017
	2a	3.006	23.7	−98.0	0.025	−96.9	14.2	0.025	0.015
						−93.8	9.2	0.025	0.017
	2b	3.551	21.8	−184.3	0.027	−174.9	10.3	0.027	0.016
						−151.2	4.0	0.027	0.018
	2c	5.260	50.7	−184.0	0.027	−173.7	38.7	0.027	0.017
						−148.1	32.4	0.028	0.018
	3a	3.428	21.9	−184.4	0.026	−172.1	10.9	0.026	0.016
						−148.5	4.5	0.026	0.018
	3b	3.043	22.0	−96.8	0.026	−96.2	12.6	0.026	0.016
						−93.1	7.6	0.026	0.017
	3c	4.595	50.0	−99.2	0.026	−96.4	40.1	0.026	0.016
						−92.2	34.7	0.026	0.017
	3d	4.595	50.2	−186.0	0.024	−171.7	38.7	0.024	0.015
						−145.5	32.4	0.024	0.016
MLI-B	2a	3.006	14.3	−101.4	0.028	−100.9	1.1	0.028	0.019
						−93.5	−9.0	0.029	0.023
	2b	4.087	21.4	−184.6	0.031	−170.6	5.2	0.031	0.021
						−137.7	−8.0	0.032	0.026
	2c	6.011	50.2	−184.4	0.031	−168.9	34.4	0.031	0.020
						−132.5	21.7	0.032	0.025
MLI-C	1a	3.450	21.8	−186.6	0.026	−168.9	15.4	0.026	0.026
						−126.4	−7.9	0.027	0.040
	1b	5.035	56.6	−186.4	0.024	−163.4	51.4	0.024	0.024
						−116.4	28.5	0.025	0.034
	1c	4.686	56.4	−102.2	0.024	−100.5	51.5	0.024	0.024
						−84.8	32.2	0.025	0.032
	1d	3.003	24.3	−104.2	0.024	−104.4	18.1	0.024	0.024
						−92.7	−2.0	0.025	0.036
MLI-D	3a	1.200	21.9	−187.5	0.009	−171.6	20.3	0.009	0.005
						−144.6	13.9	0.009	0.005
	3b	1.228	21.9	−98.4	0.010	−101.3	20.0	0.010	0.006
						−97.1	13.8	0.010	0.006
	3c	2.101	49.4	−103.6	0.012	−100.7	47.2	0.012	0.006
						−95.8	40.1	0.012	0.007
	3d	1.951	53.1	−186.4	0.010	−164.9	50.7	0.010	0.005
						−143.5	42.5	0.010	0.006

[a]Areas involved in the tests and computation: A_{hwr} = 0.314 m², A(MLI-A) = 0.597 m², A(MLI-B) = 0.597 m², A(MLI-C) = 0.343 m², and A(MLI-D) = 0.597 m².
[b]Each test phase has two data lines. T_o and T_i are center-averaged for the first data line and corner-averaged for the second data line.

is based on A(MLI), which is equal to 0.597 m² except for MLI-C. When the underlying area is made the same, the physical argument presented in the preceding paragraph would be borne out. As a matter of fact, A(MLI-C) is equal to 0.343 m², which is quite a bit closer to A_{hwr} than A(MLI-A); one sees that $\varepsilon_{\text{eff-hs}}$ is indeed smaller than $\varepsilon_{\text{eff-io}}$ in this case. This points out another important consideration that is not always clear to the analyst. When modeling by the scheme shown in Fig. 1c, it is A(MLI) that should be used in conjunction with an A(MLI)-based $\varepsilon_{\text{eff-io}}$. But when modeling by the scheme shown in Fig. 1b, one must use A_{hwr}, and one must make sure that the $\varepsilon_{\text{eff-ho}}$ value derived from a certain hardware dimension is applicable to the modeled configuration. The (22.86 cm)³ box employed in these tests is representative of many of the instrument sizes for the Cassini spacecraft, but blind application of the Table 1 data is strongly warned against.

Note that in Table 1, whether T_o and T_i are center- or corner-averaged does not seem to make a large difference when computing $\varepsilon_{\text{eff-io}}$ for MLI-A and MLI-D. However, the difference shows for MLI-B, and especially for MLI-C. This is because corner temperatures vary widely, perhaps because of the varying condition of contact with the hardware (recalling that MLI-C is a snug fit). More importantly, ΔT between the center-averaged and corner-averaged temperatures is much greater for MLI-C than for MLI-A (e.g., 23°C vs 6°C for T_i, and 47°C vs 25°C for T_o). Details of heat loss at and near the seams become important and the averaging of corner temperatures is no longer meaningful. Therefore, while values of $\varepsilon_{\text{eff-io}}$ for MLI-B and MLI-C as presented in Table 1 offer a glimpse of the location dependency of effective emittance and a hint of the range of variation, a better understanding of the MLI heat loss mechanism involved is essential.

Heat Loss in the Vicinity of Seams

The revelation of the dramatic difference between the center and corner temperatures and of the heat loss characteristics in the vicinity of seams came as a bonus. The unexpectedly large center-corner ΔT as discussed previously suggested that something might be learned by placing additional thermocouples on the test articles in subsequent test phases, over the inner- and outer-layer surfaces, and especially along the seams. The details of a typical seam and corner for the Cassini MLI blankets are shown in Fig. 6. Note that the open flap is to be closed with a Nomex lacing through the edge holes. This is a typical construction for JPL spacecraft MLI over the decades.

Figure 7 exemplifies the temperature distribution across a blanket surface, from seam-to-seam. Note that on the blanket inner layer, the temperature at the seam is more than 30°C

lower than in the middle, while on the outer layer, the seam temperature is higher than that at the center by more than 70°C. These differences are more accentuated than indicated in Table 1 because the corner thermocouples were located at some distance away from the seams. It is reasoned that, at the seam, the stitches pinch the MLI layers together and cause a thermal short; this brings the outer- and inner-layer temperatures closer to each other at the seam more than anywhere else.

Utilizing the outer-layer temperatures and emissivity, and the shroud temperature and emissivity, the local heat losses were computed, and the results are presented in Fig. 8 as a function of distance from the left seam. The heat loss varies from less than 3 W/m^2 at the center to almost 30 W/m^2 at the seam, based on A(MLI). With the understanding that in-layer heat transfer is negligible compared to the outflow normal to the MLI (as can be verified by calculation), local effective emittance (i.e., $\varepsilon_{\text{eff-io}}$) was then calculated using the inner- and outer-layer temperatures and the heat losses of Fig. 8. The results are plotted in Fig. 9, where it is seen that local effective emittance varies from a low of 0.006 to a high of almost 0.15.

The average effective emittance must lie somewhere in between, depending on the size of the blanket, and other hardware configuration parameters. The larger the blanket, the more the low emittance in the middle will weigh on the average. It is clear that, in selecting a value for the MLI effective emittance, analysts must consider the size and other geometric factors of the MLI, and how the MLI will be fabricated and assembled. Figure 9 gives suggestions as to the upper and lower bounds of effective emittance that one may select in conducting sensitivity studies, as well as points to a way of improving MLI thermal performance; i.e., by minimizing the seam losses. For a small box such as used in these tests, Fig. 8 clearly shows the importance of heat losses in the vicinity of seams. If seam losses are minimized by avoiding through seams, then the performance of the MLI can be substantially improved. The 2.6-fold reduction of effective emittance exhibited by MLI-D, as pointed out earlier, proves the point.

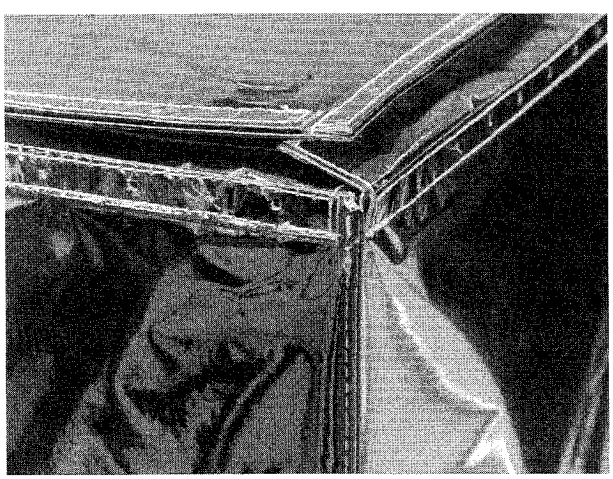

Fig. 6 MLI seam and corner construction.

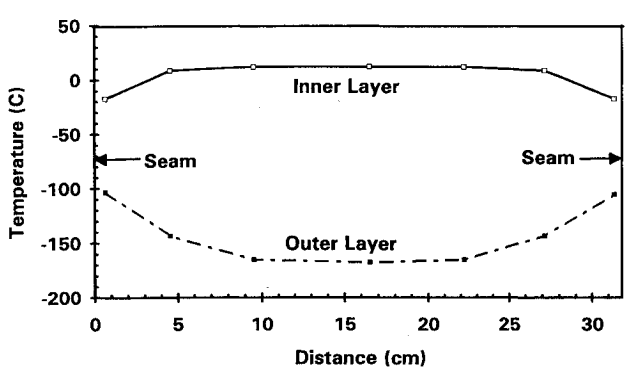

Fig. 7 MLI-A inner- and outer-layer temperature distribution.

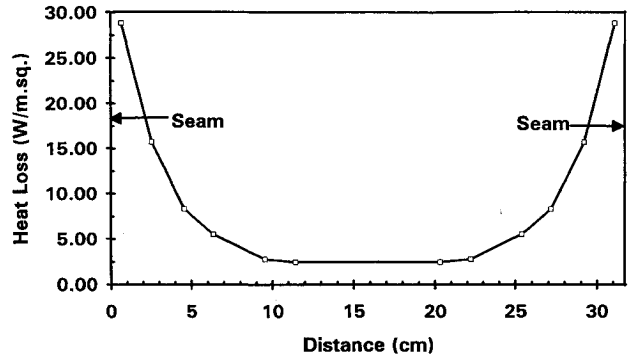

Fig. 8 MLI-A heat loss distribution.

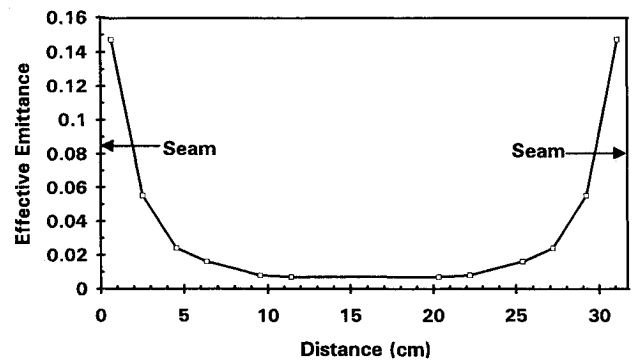

Fig. 9 MLI-A local effective emittance.

Conclusions

The Kapton–Mylar hybrid layup and the all-Kapton high-temperature layup are designed to respond to the high-temperature environments that the Cassini spacecraft will encounter in its mission to Saturn. Thermal development tests have been conducted to characterize their effective emittance and verify that these MLI designs can provide adequate thermal performance. The test results have yielded effective emittance for four different MLI layups/configurations at several temperature settings. These results have high repeatability and are amenable to consistent physical interpretations.

The all-Kapton layup was shown to be leakier (19% higher effective emittance) than the hybrid layup, bearing out a long-held intuitive conjecture. The MLI fabricating technique of duo-layup and staggering seams has been applied to enhance blanket performance over the years, but these tests gave the first quantitative proof that the technique does work, and with a dramatic 2.6-fold performance gain.

Attention has been called to the distinction between three effective emittance definitions, all having relevance to Cassini hardware–MLI configurations. The intrinsic effective emittance $\varepsilon_{\text{eff-io}}$ should be used in situations where the MLI drapes over the hardware in a tent-like manner (e.g., the PMS and FPP). On the other hand, the traditional effective emittance $\varepsilon_{\text{eff-hs}}$ (or more accurately $\varepsilon_{\text{eff-ho}}$), should be applied where the MLI wraps around the hardware snugly or is spaced off by the micrometeoroid standoffs.

The observation of large temperature differences between the center and seam of a blanket (up to 70°C) was unexpected. But a follow-up investigation led to a welcome revelation of the heat loss characteristics in the vicinity of seams. The quantitative results obtained on temperature distribution over a blanket surface, and location dependency of heat loss and ef-

fective emittance, shed light on a major MLI heat loss mechanism. They offer a guide for thermal analysts in conducting sensitivity studies, and explain the superior performance of the duo-layup, staggered-seam MLI construction.

Acknowledgments

The work described in this paper was carried out by the Jet Propulsion Laboratory, California Institute of Technology, under a contract with NASA, NAS7-1260. The authors appreciate the cooperation and assistance provided by the following individuals during the course of the tests: J. Real, R. Martinez, A. Burrows, T. Fisher, P. Martin, G. Laugen, E. Bailey, D. Perry, R. Okamoto, L. Johnson, and H. Winter. P. Stevens measured the optical properties, M. Greenfield contributed some cogent remarks, and K. Juanero and J. van Lepp helped plot the figures.

References

[1]Doenecke, J., "Survey and Evaluation of Multilayer Insulation Heat Transfer Measurements," 23rd International Conf. on Environmental Systems, SAE International, The Engineering Society for Advancing Mobility Land Sea Air and Space, Warrendale, PA, July 1993.

[2]Tien, C. L., and Cunnington, G. R., "Radiation Heat Transfer in Multilayer Insulation Having Perforated Shields," AIAA Paper 73-718, July 1973.

[3]Stimpson, L. D., and Jaworski, W., "Effects of Overlaps, Stitches, and Patches on Multilayer Insulation," AIAA Paper 72-285, April 1972.

[4]Lin, E. I., and Stultz, J. W., "Cassini Multilayer Insulation Blanket High-Temperature Exposure Tests," *Journal of Thermophysics and Heat Transfer*, Vol. 9, No. 4, 1995, pp. 778–783.